JOURNAL OF GEOPHYSICAL RESEARCH, VOL. 103, NO. B6, PAGES 12,495–12,509, JUNE 10, 1998

# Further structural constraints and uncertainties of a thin laterally varying ultralow-velocity layer at the base of the mantle

Edward J. Garnero
Berkeley Seismological Laboratory, University of California, Berkeley

Donald V. Helmberger
Seismological Laboratory, California Institute of Technology, Pasadena

**Abstract.** Constraints and uncertainties are presented for modeling of an ultralow-velocity zone layer (ULVZ) at the base of Earth's mantle using an *SKS* wave with small segments of *P* wave diffraction at the *SKS* core entry and exit locations, called $SP_dKS$. Source or receiver effects are ruled out as causes for the $SP_dKS$ anomalies used to map ULVZ structure, since systematic $SP_dKS$-*SKS* travel time moveout behavior is present in profiles of recordings of a given earthquake at many seismographic stations and also for many events recorded at one station. The southwest Pacific region produces strong variability in observed $SP_dKS/SKS$ amplitude ratios (compared to synthetic seismograms), which geographically corresponds to an anomalous ULVZ region. Accurate determination of absolute ULVZ thicknesses requires knowledge of, in addition to magnitude of *P* wave velocity ($V_P$) reduction in the layer, the magnitude of *S* wave velocity ($V_S$) reduction and density (ρ) perturbation (if any). Synthetic seismogram experiments demonstrate several key points regarding uncertainties and constraints in modeling ULVZ structure: (1) thicker layers (up to 300 km thick) with mild reductions (e.g., -2.5 to -5.0%) cannot reproduce the anomalous $SP_dKS$ behavior seen in the data; (2) for ULVZ layers less than 10 km thick, strong trade-offs exist between discontinuous velocity reductions and linear gradient reductions over a thicker zone; (3) uncertainties preclude precise determination of magnitude of $\delta V_P$ and $\delta V_S$ reductions, as well as the $\delta V_S$:$\delta V_P$ ratio; (4) large density increases within the ULVZ (e.g., up to 60% and more) can efficiently broaden and delay the peak of the energy that we identify as $SP_dKS$ for models with strong velocity reductions in the layer; (5) models with extreme *Q* reductions in the ULVZ can affect $SP_dKS$ waveforms, and dampen spurious ringing energy present in *Sd* waveshapes due to the ULVZ; and (6) the minimum required $V_P$ reduction for the most anomalous data (around -10%) trades off with thinner ULVZ structures containing larger velocity reductions (with possible density increases as well).

## 1. Introduction

The core-mantle boundary (CMB) is a boundary between very different environments and continues to attract active research efforts from many different geophysical disciplines (see *Lay et al.* [1998] for a review). The CMB is a chemical, phase, and thermal boundary layer, and it is intimately linked to, for example, mantle and core material circulation mechanisms, heat flux across the CMB in the cooling of the core, and the behavior of the Earth's magnetic field. Seismology has been an effective remote sensing tool in imaging layering in the deep Earth and lateral variations in properties; further resolving structural issues associated with the CMB can enable us to better understand both the small- and large-scale dynamics of the region.

This paper addresses uncertainty issues associated with the identification of a thin (<40 km) ultralow-velocity zone (dubbed "ULVZ", with *P* wave velocity reductions of 10% or more) at the base of the mantle (see *Garnero et al.* [1998] for a summary of ULVZ studies and associated interpretations). This layer has been investigated using various seismic phases: the $SP_dKS$ phase, which is an *SKS* wave that has short segments of CMB mantle-side *P* wave diffraction at the *SKS* core entry and exit locations (see Figure 1) [*Garnero and Helmberger*, 1995, 1996, hereinafter denoted as GH95 and GH96, respectively; *Helmberger et al.*, 1996a, b; *Fischer et al.*, 1996; D.V. Helmberger et al,. Deep ultralow velocity structure beneath Iceland, submitted to *Nature*, 1998, hereinafter referred to as Helmberger et al., submitted manuscript, 1998; L. Wen and D.V. Helmberger, A two-dimensional *P-SV* hybrid method and its applications to modeling the *SKS-SPdKS* phases from ultralow-velocity zone at the core-mantle boundary, submitted to *Journal of Geophysical Research*, 1998, hereinafter referred to as Wen and Helmberger, submitted manuscript, 1998]; precursors to the core-reflected *PcP* phase, due to the large contrast in properties at the top of the ULVZ [*Mori and Helmberger*, 1995; *Revenaugh and Meyer*, 1997]; and precursors to the core-reflected *ScP* phase [*Vidale et al.*, 1995].



Paper number 98JB00700.
0148-0227/98/98JB-00700$09.00

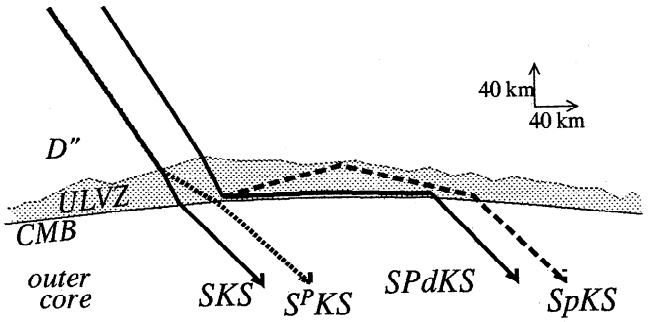


**Figure 1.** Diagram showing *SKS*, $SP_dKS$, $S^PKS$, and *SpKS* ray paths in vicinity of CMB, with an ultralow-velocity zone (ULVZ) present.

Studies of International Seismological Centre arrival time data have also argued for a thin (20 km) boundary layer having velocity perturbations of ±10% and greater [e.g., *Doornbos and Hilton*, 1989; *Sylvander and Souriau*, 1996; *Sylvander et al.*, 1997]. While low velocities in such studies are conceptually identical to the recently proposed ULVZ structure, trade-offs are present between velocity perturbations and the thickness of the layer [e.g., see *Doornbos and Hilton*, 1989]. Many studies have imaged seismic velocities in the lowermost few hundred kilometers of the mantle, particularly at long wavelength, without identification of ultralow velocities. Typical magnitude of D″ heterogeneity in tomographic studies is ±2-3% [e.g., *Su et al.*, 1994; *Wysession*, 1996a; *Grand et al.*, 1997]. However, methods that utilize travel times of seismic waves that vertically average D″ structure (such as *PcP*, *PKP*, and long-period diffracted *P* waves, $P_d$) may have mapped ULVZ signal into more dispersed lower mantle structure, or reductions in the lower mantle one-dimensional (1-D) profile (e.g., *Song and Helmberger* [1995] noted the need for a reduced $V_P$ in the lowermost mantle to explain observed time separations of different *PKP* phases).

Recent ULVZ studies have provided inference for a low-velocity boundary layer with lateral variations in thickness (Figure 1), such as beneath the central Pacific, Africa, and Iceland [see *Garnero et al.*, 1998]. The origin of the ULVZ may be due to partial melt, a change in chemistry, or a phase change, though arguments for the presence of liquid in the lowermost mantle as the most dominant explanation have been recently put forth [*Williams and Garnero*, 1996; *Garnero et al.*, 1998]. High-pressure mineral physics experiments corroborate the feasibility of melt at the base of the mantle [*Holland and Ahrens*, 1997]. Thus lateral thermal gradients may directly relate to the layer's thickness and existence. Chemical heterogeneity in the ULVZ with possible origin from chemical reactions between the mantle and core [*Knittle and Jeanloz*, 1989] can also be an important component of the ULVZ layer [*Manga and Jeanloz*, 1996].

A ULVZ environment having laterally localized higher-than-average temperatures in the lowermost mantle may be dynamically linked to upwelling motions, including plumes [e.g., *Olson et al.*, 1987; *Hansen and Yuen*, 1988; *Kellogg and King*, 1993], with other phenomena, such as viscous heating in the bottom portion of upwelling plumes [e.g., *Zhang and Yuen*, 1996] possibly playing an important role. A ULVZ containing partial melt with low viscosity would likely be closely related to such features, including its possible relationship to the genesis of mantle plumes and hot spots (Q. Williams et al., A correlation between ultra-low basal velocities in the mantle and hot spots, sumitted to *Science*, 1998, hereinafter referred to as Williams et al., submitted manuscript, 1998) and also the reversal of the Earth's magnetic field along preferred paths [*Aurnou et al.*, 1996]. Thus the intimate relationship between a low-velocity boundary layer at the base of the mantle and phenomena from related geophysical disciplines warrants further investigation of its structural details and uncertainties.

In this paper, we further analyze $SP_dKS$ behavior of data and synthetic predictions, in order to (1) rule out source or receiver structure as explanations for the anomalous $SP_dKS$ behavior that has been previously noted as due to a ULVZ; (2) show lateral scale lengths of strong variability within the ULVZ may be <50-100 km in the most anomalous region of the southwest Pacific study area; (3) document geographical systematics in anomalously large $SP_dKS$ amplitudes; (4) discuss structural issues relating to the large $SP_dKS$ amplitudes and times; and (5) discuss trade-off issues in the modeling parameter space, which arise when other free parameters in the modeling are considered, such as large $V_S$ reductions and density (ρ) increases, gradient versus discontinuity structures, and strong attenuation.

## 2. $SP_dKS$ Data

### 2.1. Background

The discovery of the $SP_dKS$ phase was first made from theoretical wave propagation studies [*Kind and Müller*, 1975; *Choy*, 1977; *Aki and Richards*, 1980]. $SP_dKS$ waves are due to an *SKS* wave near 107° in epicentral distance (a model dependent distance), which has an angle of incidence to the CMB that is the critical angle for *ScP* waves. At this ray parameter, *SKS* energy converts to diffracted *P* wave energy along the mantle side of the CMB. This leaking of *SKS* energy into short segments of *P* wave diffraction occurs at the *SKS* core entrance and exit locations. Since *SKS* and $SP_dKS$ travel nearly identical mantle paths, $SP_dKS$ delays relative to *SKS* cannot be explained solely by anomalous D″ or lower mantle $V_S$ structure. For example, at 110°, a diagnostic distance for identifying anomalous $SP_dKS$ behavior, *SKS* and $SP_dKS$ ray paths are separated by only 150 km at the CMB. Thus mantle-side CMB *P* wave velocity reductions must be invoked, which delays $P_d$ segments in $SP_dKS$.

A summary of ULVZ studies and interpretation of possible origins of the ULVZ are given by *Garnero et al.* [1998]. Beneath the central Pacific, ULVZ structure is overlain by laterally varying low *S* wave velocities (up to a few percent) over a wide range of scale lengths [*Schweitzer*, 1990; GH95; *Sylvander and Souriau*, 1996; *Su et al.*, 1994; GH96; *Grand et al.*, 1997; also *Ritsema et al.*, 1997]. In contrast to the central Pacific, data having circum-Pacific wave path geometries are easily explained by structures in absence of a ULVZ; such data are well-modeled by predictions from standard 1-D reference Earth models [GH96].

### 2.2 Geographical Systematics

The contrasting central versus circum-Pacific $SP_dKS$ behavior for a compilation of long-period radial component World-Wide Standardized Seismographic Network (WWSSN) data is shown in Figure 2. The map in Figure 2a shows the CMB $P_d$ segments (thick lines) in $SP_dKS$ wave paths for the

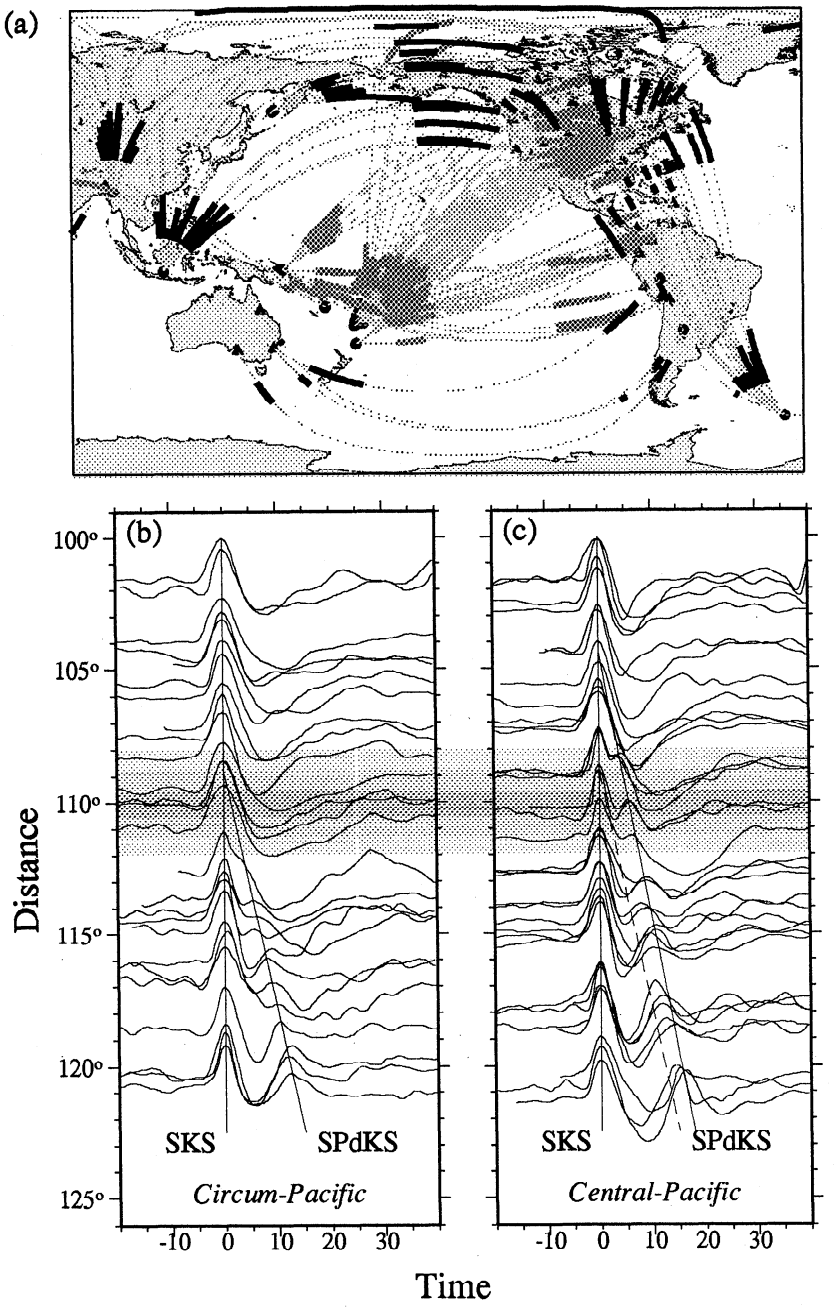


**Figure 2.** (a) Map showing great circle paths (thin shaded lines) for events (circles) and stations in and around the Pacific. $P_d$ segments of $SP_dKS$ are shown as thick solid (circum-Pacific) and shaded (central Pacific) line segments. (b) Circum-Pacific WWSSN longitudinal component *SKS* and $SP_dKS$ data. Lines demark *SKS* and $SP_dKS$ peaks as predicted by PREM. (c) Central Pacific WWSSN longitudinal component *SKS* and $SP_dKS$ data. Solid lines are for *SKS* peaks and average observed $SP_dKS$ peaks; dashed line corresponds to the PREM predicted $SP_dKS$ delay, as in Figure 2b. Shaded region in Figures 2b and 2c corresponds to the distance range of easily identifiable $SP_dKS$-*SKS* differences between the two profiles. Data are normalized in time and amplitude to the *SKS* phase.

two geometries. The data of circum-Pacific paths are shown in Figure 2b, along with lines for predictions from the preliminary reference Earth model (PREM) [*Dziewonski and Anderson*, 1981]. The $P_d$ arcs for the data in Figure 2b are the thick solid lines in the map of Figure 2a. The timing of $SP_dKS$ relative to *SKS* for these data is well-predicted by the PREM model as displayed in GH96. For these data (and PREM), $SP_dKS$ energy initiates near 108° and is first identifiable near 111°, appearing as a broadened pulse, and then more obviously as a secondary pulse at 113°. Figure 2c displays the $SP_dKS$ data for wave path geometries crossing the central Pacific (thick shaded line segments in the map of Figure 2a). The $SP_dKS$ phase is easily identifiable as a secondary pulse at 109° and beyond, several degrees earlier in distance than that of circum-Pacific data. This is easily seen when comparing the shaded distance window of Figures 2b and 2c: in contrast to the single arrival for circum-Pacific data, the central Pacific data display $SP_dKS$ fully developed as a secondary arrival. Several interesting

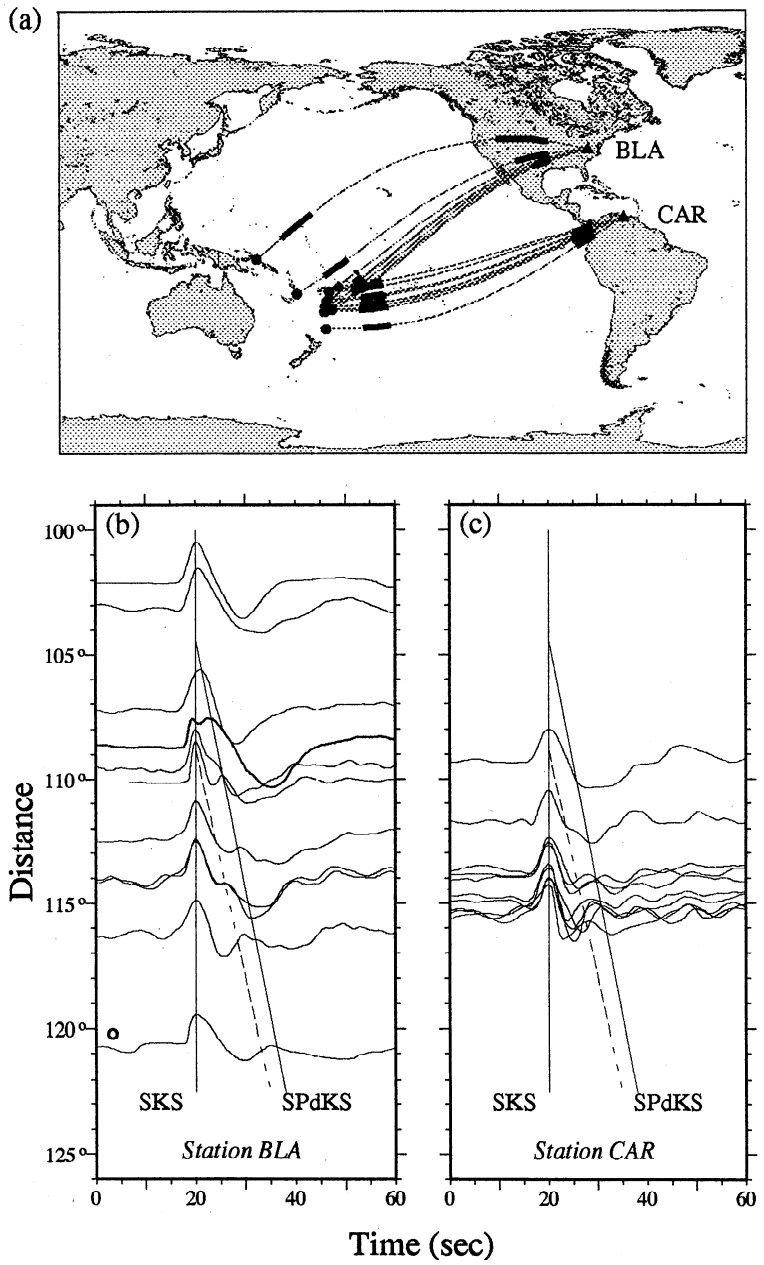


**Figure 3.** (a) Map showing great circle paths (thin shaded lines) for southwest Pacific events (circles) and stations BLA and CAR (triangles). $P_d$ segments of $SP_dKS$ are shown as thick solid line segments. (b) *SKS* and $SP_dKS$ WWSSN longitudinal component data recorded at BLA. (c) *SKS* and $SP_dKS$ WWSSN longitudinal component data recorded at CAR. Data are normalized in time and amplitude to the *SKS* phase.

features are present for the data of Figure 2c: (1) several seconds of delay in $SP_dKS$ (secondary peak in data, demarked by rightmost solid line) relative to PREM predictions (dashed line); (2) several seconds of variability in $SP_dKS$ arrival time (in some cases at a given distance); and (3) larger $SP_dKS/SKS$ amplitude ratios than for circum-Pacific data having similar $SP_dKS$ delays: shifting the circum-Pacific record (e.g., from 114°) to smaller epicentral distance (e.g., 109°) is necessary for such a comparison. The presence of strong velocity reductions in a ULVZ retards the $SP_dKS$ arrival time and enhances its amplitude, explaining features 1 and 3, respectively, and strong lateral variations in ULVZ properties can explain feature 2. These issues are further explored in the following sections.

There is some overlap in the $P_d$ segments in $SP_dKS$ data from the normal and anomalous geometries (Figures 2b and 2c, respectively, see also GH96), especially when the $P_d$ Fresnel zones are considered [*Garnero et al.*, 1998]. However, this overlap is only partial; hence uncertainty is present when interpreting $SP_dKS$ anomalies from the Fiji-Tonga → North America corridor as solely being due to ULVZ structure in the southwest Pacific. Nonetheless, if a ULVZ exists in the regions sampled by the north-south paths underneath the Americas, its thickness is less than a few kilometers, or the data of Figure 2b would display $SP_dKS$ anomalies, in contrast to the observations. Hereinafter, we assume that the anomalies in $SP_dKS$ data traversing the central Pacific are due to ULVZ

structure on the source-side of the $SP_dKS$ path, i.e., in the southwest Pacific. While this assumption is not well-constrained, we note that no $SP_dKS$ data with north-south paths beneath the Americas display any anomaly whatsoever.

Complex receiver structure and/or complicated earthquake source-time history can cause secondary arrivals in seismic phases. Distance profiles of data (such as that in Figure 2) help in distinguishing between the travel time behavior of arrivals of interest and receiver or source effects. Station profiles in particular (many events recorded at one station) are also useful in establishing the stability (or instability) of $SP_dKS$ behavior. Examples of such are presented in Figure 3a, 3b, and 3c. Available records from 13 events recorded at station BLA (Blacksburg, Virginia; Figure 3b) and CAR (Caracus, Venezuela; Figure 3c) show systematic $SP_dKS$ moveout relative to $SKS$. Data recorded at BLA have wavepaths that cross the most anomalous region of the ULVZ of GH96; many $SP_dKS$ arrivals at this station are coincident in time to the average of the central Pacific compilation of Figure 2c (rightmost solid line in Figure 3b). The lack of any secondary arrival at a constant delay time after $SKS$ in the BLA profile argues against any significant receiver structure contribution to misidentification of $SP_dKS$. Also contributions to secondary arrivals due to source effects for these data are ruled out from analyses of many stations for each event. Some of the BLA data have $SP_dKS$ arrivals between the PREM line (dashed) and the anomalous data line, indicating lateral variations in ULVZ properties. To deterministically model these variations, however, contributions to the anomaly from the source- or receiver-side ULVZ must first be sorted out. Nonetheless, some trends are apparent: the two most northerly paths (which correspond to the largest distances, Figure 2c) are the least anomalous, suggesting a relatively thinner ULVZ (or one with less anomalous properties) for those paths. Similarly, the two records at 114° display PREM-like $SP_dKS$ behavior, indicating the presence of strong lateral variations in this study area.

A station profile for CAR is displayed in Figure 3c. $SP_dKS$ arrivals for this profile have variable arrival times between the PREM prediction and the anomalous data average (dashed and solid lines, respectively). This is consistent with a laterally variable ULVZ having thickness (or anomalous properties) slightly less than that sampled by the BLA data (e.g., view records for both stations between 109° and 113°). Possible thinning of the ULVZ to the south spatially correlates with predictions from tomographic studies of diminishing amplitudes of long wavelength low velocities in that direction (e.g., see

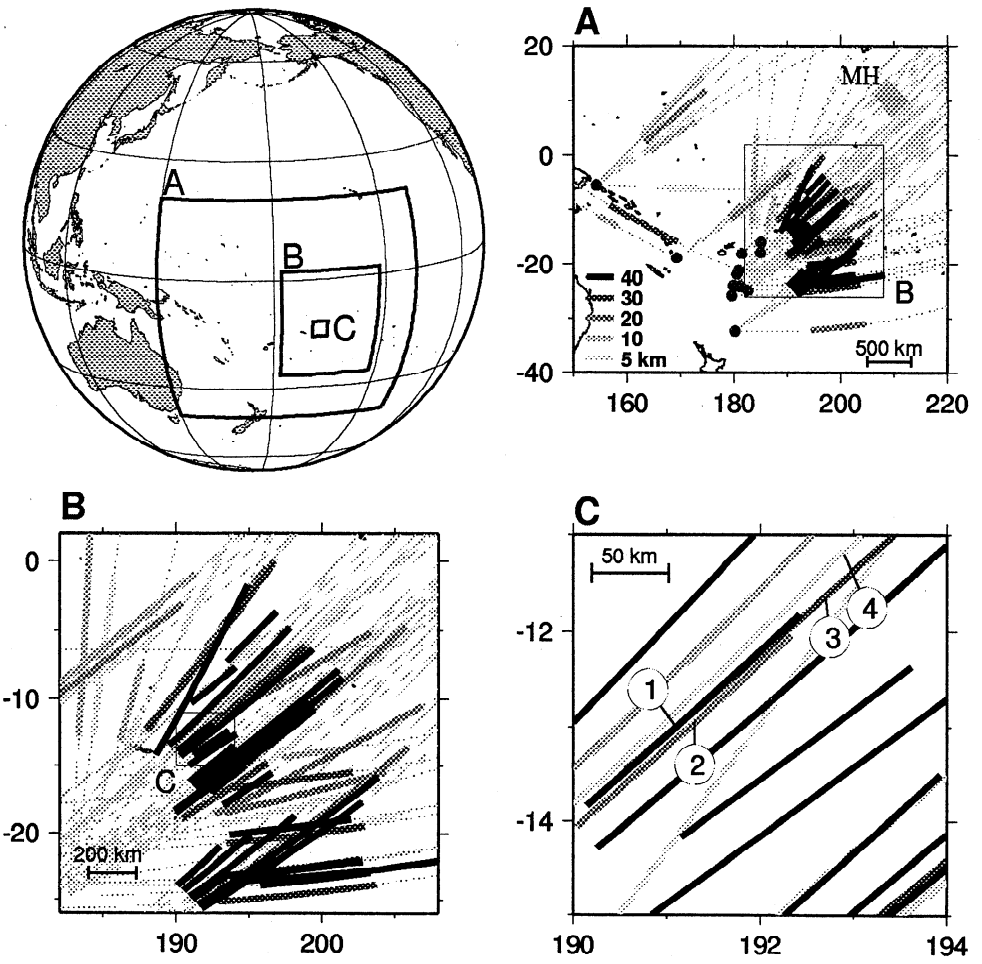


**Figure 4.** Globe showing three geographical regions: A, B, and C. Region A shows $SP_dKS$ $P_d$ segments as thick line segments shaded for corresponding ULVZ thickness; MH is region of study of *Mori and Helmberger* [1995] (adapted from GH96). Regions B and C are the same as region A but are progressively smaller areas. In region C, four $P_d$ arcs are labeled and correspond to data in Figure 5.

*Ritzwoller and Lavely* [1995] or *Wysession* [1996b] for D″ images from various tomographic studies); however, more data are needed to constrain such a trend.

For a summary of regions studied for ULVZ structure using $SP_dKS$, *PcP*, and *ScP*, see *Garnero et al.* [1998]. In the remainder of this paper we focus on details in ULVZ modeling that relate to uncertainties and trade-offs. A closer look at data used in GH96, as well as some new data, is used in conjunction with several synthetic seismogram experiments to demonstrate the presence of strong trade-offs in ULVZ modeling.

## 3. $SP_dKS$ Modeling

### 3.1. ULVZ Lateral Heterogeneity

In the $SP_dKS$ modeling of GH96, only one parameter was varied in the modeling procedure: the ULVZ thickness (from 0 to 40 km) was used to produce observed $SP_dKS$ behavior that best matched the observations. In this approach, the velocity drop in the ULVZ was fixed at $\delta V_P = \delta V_S = 10\%$, a reduction derived from forward modeling the inception of $SP_dKS$ near the distance of 108°, where $SP_dKS$ behavior is very strongly dependent on the $V_P$ reduction. This method has been quite successful in modeling most of the data, in particular, the timing of the anomalously delayed $SP_dKS$ arrivals. Closer inspection of those results reveals important information on scale length of ULVZ heterogeneity, as well as limitations of that modeling approach. Figure 4 displays a globe with three overlapping geographical regions labeled A, B, and C. Region A is the modeling result of GH96 and presents solution ULVZ thicknesses mapped to $P_d$ segments of $SP_dKS$. Also shown is the *Mori and Helmberger* [1995] study region (labeled MH); this region also coincides with the work of *Revenaugh and Meyer* [1997]. The portion of region A having thickest ULVZ estimates also displays high variability in ULVZ thickness. An enlargement of this area is given in region B (Figure 4, lower left). Here, it is more easily seen that the predominantly thick ULVZ estimates are interspersed with thinner ULVZ estimates (lighter shaded $P_d$ segments). At yet closer inspection (region C), it is apparent that data with nearly overlapping 1-D wave path geometries sometimes have quite different estimated ULVZ thicknesses (e.g., note the $P_d$ paths numbered 1 through 4 in Region C). These data along with best fitting solution synthetics from GH96 are displayed in Figure 5. The synthetics assume a ULVZ only on the source-side of the $SP_dKS$ wave path (i.e., in the southwest Pacific) and PREM on the receiver-side and were computed using a 2-D generalized ray code [*Helmberger et al.*, 1996b]. Records 1 and 2 are both at distances just beyond the inception of $SP_dKS$ (108.4° and 108.6°, respectively), while records 3 and 4 are at larger distances (117.6° and 123.3°, respectively) that correspond to much longer CMB $P_d$ segments in $SP_dKS$ (e.g., 600 and 1000 km, respectively, compared to around 100 km for records 1 and 2). The peaks of *SKS* and $SP_dKS$ are denoted by solid dots, and the data (solid traces) are overlain by synthetics (dashed traces). The records in Figure 5 provide a representative example of the range of the quality of fit to $SKS$-$SP_dKS$ waveforms using this method. In all four records, the $SP_dKS$ delay relative to *SKS* is well-reproduced. The amplitude of $SP_dKS$ compared to *SKS*, however, is highly underpredicted for record 1 and somewhat overpredicted for record 3. These records are of high quality with good signal-to-noise ratio; thus noise is not expected to play a role in the amplitude

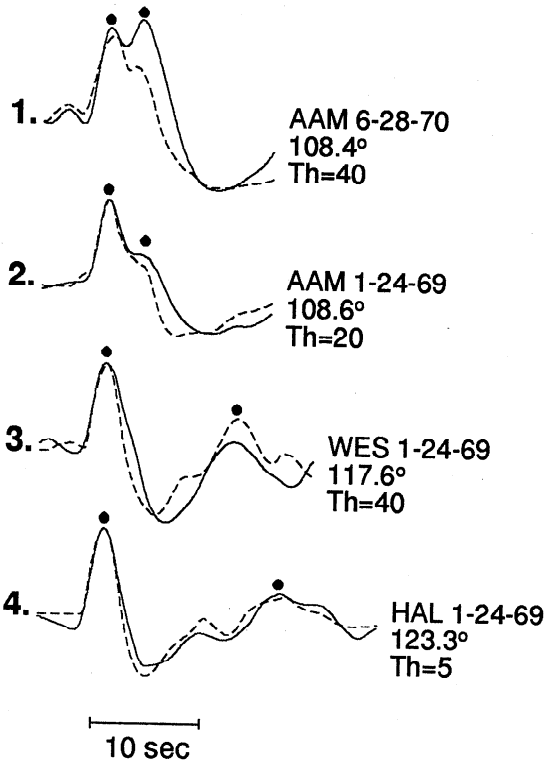


**Figure 5.** WWSSN longitudinal component data (solid) and 2-D generalized ray synthetics (dashed) for labeled $P_d$ paths (records 1-4) in region C of Figure 4. Peaks of *SKS* and $SP_dKS$ are indicated by dots.

fluctuations. While the $SP_dKS$ timing and amplitude of record 2 are adequately reproduced, the width of $SP_dKS$ is not well matched. Such a one-parameter ULVZ modeling method (i.e., only varying ULVZ thickness) for a ULVZ on just one side of the $SP_dKS$ wave path has been demonstrated as effective in modeling some profiles of data [GH96; *Helmberger et al.*, 1996a, b]. However, as Figure 5 demonstrates, this method does not account for $SP_dKS$ observations having pronounced amplitude and waveshape anomalies. Explaining these data requires further model perturbations, which may require relaxing the assumption of no receiver-side ULVZ structure. As we will show below, some significant modeling trade-offs exist when large $V_S$ reductions and ρ increases in the ULVZ are included as free parameters in the modeling procedure. ULVZ topography and/or heterogeneity can also greatly perturb the $SKS$-$SP_dKS$ behavior (see Wen and Helmberger, submitted manuscript, 1998; Helmberger et al., submitted manuscript, 1998). Nonetheless, Figures 4 and 5 demonstrate that ULVZ properties can vary at very short wavelength (< 100 km).

Utilizing the best fitting 2-D synthetics of GH96, whereby a ULVZ with 10% $V_P$ and $V_S$ reductions was varied in thickness on the source-side of the path, we calculated $SP_dKS/SKS$ amplitude ratio residuals (data divided by predictions). This calculation was carried out for the southwest Pacific data of Figure 4; only records where unambiguous amplitude ratio estimates could be calculated were retained. The results have been mapped to geographical locations of the CMB $P_d$ segments of $SP_dKS$ (Figure 6). The magnitude of amplitude ratio residuals is indicated as follows: anomalously low-amplitude ratios (<0.5, small $SP_dKS$) are solid lightly shaded

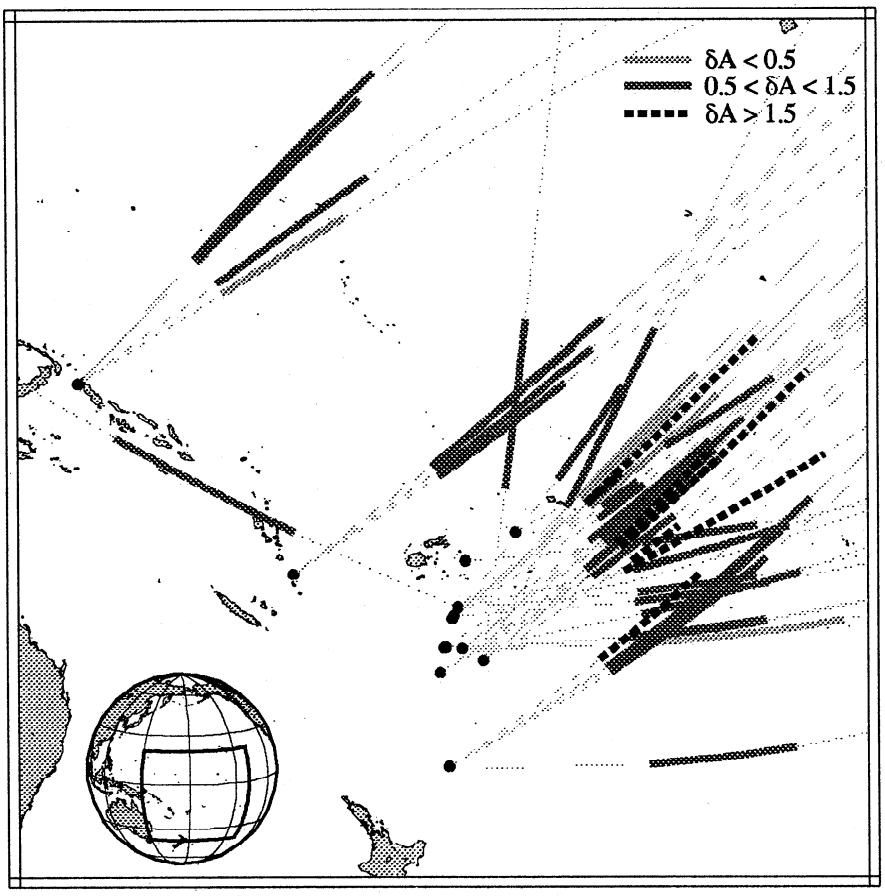


**Figure 6.** $SP_dKS$/SKS amplitude ratio residuals ( "δA", observations divided by best-fit 2-D generalized ray synthetics), shown in three groupings: anomalously large observed $SP_dKS$ arrivals (dashed $P_d$ segments), "normal" amplitudes (shaded $P_d$ segments), and anomalously small $SP_dKS$ arrivals (lightly shaded $P_d$ segments).

lines; residuals between 0.5 and 1.5 are shaded line segments; and anomalously large ratios (> 1.5, large $SP_dKS$) are dashed lines. Anomalously small and large $SP_dKS$ amplitudes are geographically coincident with the region of largest ULVZ thickness estimates in GH96 (except for one low amplitude $SP_dKS$ in the northeast of the study area). Thus any ULVZ model(s) that explain the large $SP_dKS$-$SKS$ difference times in this region must also account for highly variable $SP_dKS$/$SKS$ amplitude ratios. Owing to a wide range of factors that can possibly contribute to amplitude variability, we caution that amplitude analyses should be done through careful waveform modeling.

Some $SP_dKS$ amplitude variability can arise from introducing large shear velocity reductions and ρ increases, as we will show below. ULVZ models with 2- and 3-D structures can also perturb $SP_dKS$ amplitudes, such as a dipping ULVZ surface (which, depending on the geometry of the dip, can either amplify or destroy $SP_dKS$ energy) and also dome type structures (see Wen and Helmberger, submitted manuscript, 1998). For example, a model with a ULVZ of increasing thickness in direction of $SP_dKS$ propagation strongly amplifies (and delays) $SP_dKS$; just the opposite occurs for a ULVZ with diminishing thickness in the direction of propagation. Thus ULVZ topography can effectively reduce/enhance $SP_dKS$ amplitudes and simultaneously delay $SP_dKS$ relative to $SKS$. Nonplanar 3-D structures will surely focus/defocus $SP_dKS$ energy as well [e.g., *Hong and Helmberger*, 1978], such as concave or convex surface perturbations, or perhaps more realistic, irregular topography at the top of the ULVZ. Thus the region of anomalous ULVZ thicknesses and $SP_dKS$ amplitudes in the southwest Pacific may contain highly variable ULVZ topography.

### 3.2. ULVZ Modeling Trade-offs and Uncertainties

We now present results of several synthetic seismogram experiments that demonstrate various aspects of trade-offs and uncertainties inherent to ULVZ modeling. The 1-D reflectivity method is used for these purposes. While it is clear that ULVZ structures probed thus far exhibit strong evidence for lateral variability, the 1-D synthetic experiments still provide valuable information regarding the relative trade-off issues that have not yet been considered in ULVZ studies.

The degree of accuracy of mapping $SP_dKS$-$SKS$ times into ULVZ thicknesses using the GH96 approach depends on the ability to correctly identify $SP_dKS$ and also on accurate time picking. These issues are briefly considered here. Figure 7 displays important features of the $SP_dKS$ arrival, emphasizing the fact that strong impedance contrasts at the top of the ULVZ can efficiently trap energy in the ULVZ layer. Using $SKS$ as a reference (Figure 7a), the amplitude of $SP_dKS$ (Figure 1) can be enhanced/reduced by various choices of impedance

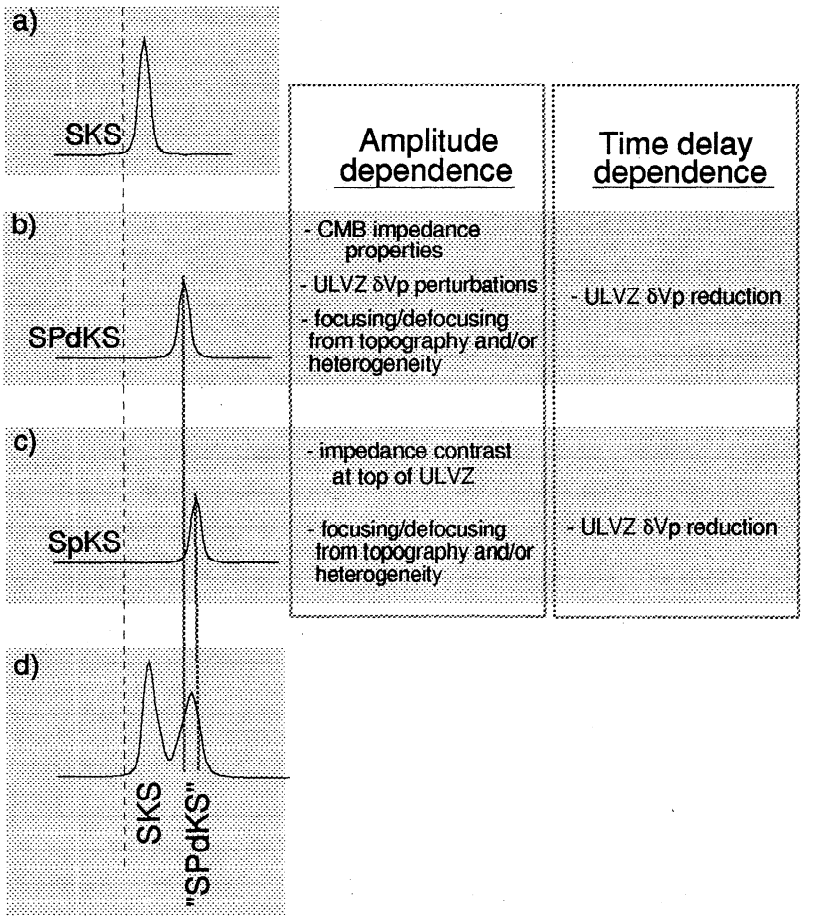


**Figure 7.** Schematic showing dependency of amplitude and timing of energy following (a) *SKS*, such as (b) $SP_dKS$, and (c) *SpKS*, which can add constructively to yield an apparently delayed $SP_dKS$ (d). See Figure 1 for ray path schematics.

properties at the top of the ULVZ and the CMB, while the time delay of the arrival is predominantly dependent on the $\delta V_P$ reduction in the layer (Figure 7b). The amplitude of *SpKS* is strongly dependent on the impedance contrast across the top of the ULVZ (Figure 7c). Any focusing/defocusing due to ULVZ heterogeneity or topography can also modulate $SP_dKS$ or *SpKS* amplitudes. If the *SpKS* energy is relatively amplified, it will broaden the pulse of combined $SP_dKS$+*SpKS* energy, thus delaying the peak of the combined arrival (Figure 7d), compared to $SP_dKS$ energy in the absence of strong *SpKS*. Figure 7 conveys the importance of considering both $SP_dKS$ and *SpKS* when interpreting the delay of the peak of the "$SP_dKS$" energy tailing *SKS*.

Synthetic seismograms computed by the reflectivity method [e.g., *Kind and Müller*, 1975; *Müller*, 1985] are utilized to assess our accuracy in time analyses of $SP_dKS$. Figure 8 displays synthetics for ULVZ models having velocity reductions $\delta V_P = \delta V_S = -10\%$ at 110°, 115°, and 120°. ULVZ thicknesses of 5, 10, 15, and 20 km are shown for each distance. Thin vertical lines are 1 s apart. When *SKS* peaks are lined up, systematic delays in $SP_dKS$ relative to *SKS* are apparent for increasing layer thickness, particularly at smaller distances. A 5-km change in ULVZ layer thickness roughly corresponds to a 1-s perturbation in $SP_dKS$-*SKS* time. A conservative bound for our uncertainty of estimated ULVZ thickness would be ±5-10 km since our difference times can easily be computed with less than ±1 s error.

One-dimensional reflectivity synthetics are used for the purpose of illustrating some of the uncertainty issues associated with added degrees of freedom in ULVZ modeling. Specifically, we have explored models with large $V_S$ drops and

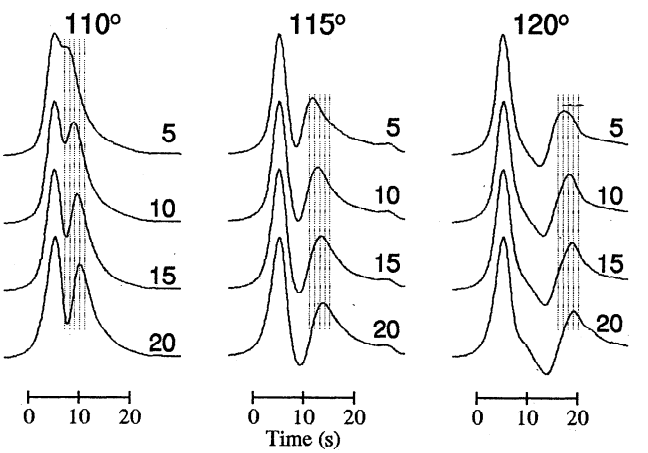


**Figure 8.** Reflectivity synthetic seismograms of *SKS* and $SP_dKS$ (first and secondary peaks, respectively) at distances 110°, 115°, and 120°, for ULVZ layer thicknesses of 5, 10, 15, and 20 km. Thin vertical lines have a 1-s spacing and illustrate that approximately ±1 s in $SP_dKS$-*SKS* timing corresponds to roughly ±5 km in estimate of ULVZ thickness.

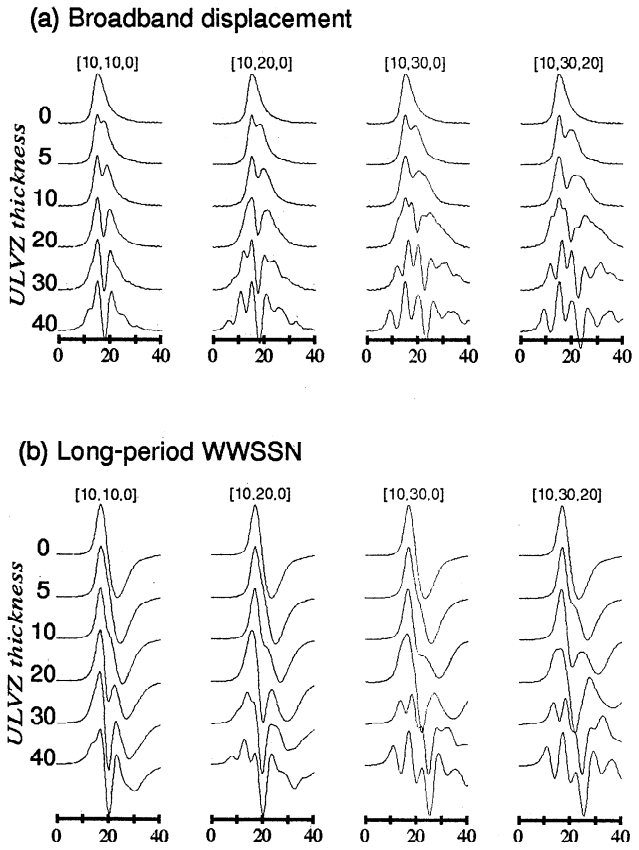


**Figure 9.** (a) Broadband displacement and (b) long-period WWSSN longitudinal component reflectivity synthetic seismograms for various ULVZ thicknesses (left column of numbers) and $V_P$ reductions, $V_S$ reductions, and ρ increases, denoted as [$\delta V_P$,$\delta V_S$,$\delta\rho$]. All synthetics are for a 500 km deep event at 110°. See text for details.

ρ increases that accompany the 10% $V_P$ drop. Larger $V_P$ reductions were also explored. Figure 9 demonstrates the effect of $V_S$ and ρ perturbations on the *SKS-SP$_d$KS* wave group. All synthetics in Figure 9 are for 110° and a source depth of 500 km. This particular distance is displayed because of its utility as a diagnostic for anomalous *SP$_d$KS* behavior, as discussed earlier. Broadband and long-period WWSSN synthetics are shown (Figure 9a and 9b, respectively) for ULVZ thicknesses of 0 (PREM), 5, 10, 20, 30, and 40 km (left column of numbers). Synthetics corresponding to $V_S$ reductions of 10, 20, and 30%, as well as a 30% $V_S$ reduction with a 20% ρ increase are shown (all having a 10% $V_P$ reduction). The nomenclature [$\delta V_P$ (reduction), $\delta V_S$ (reduction), δρ (increase)] is displayed above each column of synthetics. Large $V_S$ reductions retard and broaden the *SP$_d$KS* arrival (e.g., compare the [10,30,0] and [10,10,0] broadband synthetics for a 10 km thick ULVZ); large ρ increases add to this effect. This is due to increasing the amplitude of the *SpKS* phase, which effectively broadens the peak of the composite *SP$_d$KS-SpKS* arrival (as stated in Figure 7). Additional arrivals are present for the thicker ULVZ estimates, resulting in complex motions, especially for models with large $V_S$ reductions. The additional energy is due to a series of mode conversions and internal reflections within the ULVZ, due to the large contrast in elastic properties between the ULVZ and the overlying mantle. For instance, large $V_S$ reductions increase the amplitude of the *S*-to-*P* mode conversion of downgoing *SKS* waves encountering the top of the ULVZ, resulting in a significant *SKS* precursor (*S$^P$KS*, Figure 1). Additional multiple reflections within the ULVZ layer also strongly develop (e.g., *SpKS*, Figure 1, as well as higher multiples), ultimately causing *SKS* and *SP$_d$KS* to appear as a wave group of many arrivals. Energy from these arrivals is also contained in the thinner (simpler waveform) ULVZ synthetics but has not dispursed into separate detectable arrivals (due to the smaller layer thickness). We will discuss two aspects of Figure 9: predictions from a ULVZ model having $\delta V_P$=-10%, and little or no $V_S$ reduction can be assimilated by a thinner ULVZ with $\delta V_P$=-10% and a large $V_S$ depression (and possibly a ρ increase); and the complications seen for the thick ULVZ predictions with large $V_S$ decreases are incompatible with observations for the central Pacific wave path geometry.

For selected records in Figure 9, nearly identical *SP$_d$KS-SKS* separations are present for models having differing ULVZ thicknesses (in some cases waveforms are nearly identical) because of trade-offs with $V_S$ reductions and ρ increases. This is illustrated in Figure 10, which displays WWSSN synthetics taken from Figure 9b. In Figure 10a, a prediction from a 20 km thick ULVZ having 10% reductions in $V_P$ and $V_S$ are compared to that for a 10 km thick ULVZ with 10% and 30% $V_P$ and $V_S$ reductions, respectively. These synthetics illustrate the case where *SP$_d$KS-SKS* times are in agreement, but the *SP$_d$KS/SKS* amplitude ratios are not. Figure 10b compares a 10 km thick ULVZ having a 10% reduction in $V_P$, 20% in $V_S$, to one that is 5 km thick, possessing a 10% reduction in $V_P$, 30% in $V_S$, and a 20% increase in ρ. These records are nearly identical in *SKS-SP$_d$KS* differential timing and waveshape. Such trade-offs producing identical records only occurs for ULVZ structures with thicknesses less than around 20 km; otherwise, *SKS* precursors (*S$^P$KS*) and *SKS+SP$_d$KS* multiples (e.g., *SpKS*) within the ULVZ layer produce diagnostic waveshapes that help to distinguish between models. As we will show shortly, thinner ULVZ layers containing even more extreme ($\delta V_P$,$\delta V_S$,δρ) perturbations further expand the trade-off space.

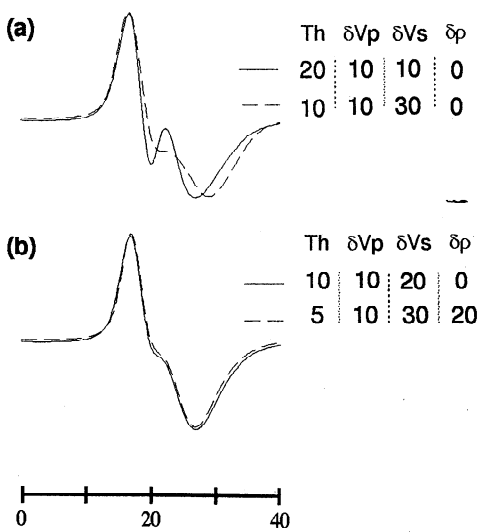


**Figure 10.** Comparison of WWSSN synthetics from Figure 9: (a) two synthetics displaying similar *SP$_d$KS-SKS* separations, with disparate *SP$_d$KS/SKS* amplitude ratios for ULVZ structures with properties given to the right; and (b) two synthetics with nearly identical *SP$_d$KS-SKS* behavior for the ULVZ properties shown to the right.

The partial melt hypothesis of *Williams and Garnero* [1996] as the origin of the ULVZ predicts 30% $V_S$ reductions associated with 10% $V_P$ reductions (more specifically, a 3:1 $\delta V_S$:$\delta V_P$ ratio). If such $V_S$ reductions are adopted to accommodate the partial melt scenario, then a $SP_dKS$-$SKS$ anomaly previously explained by a ULVZ with solely a 10% reduction in both $V_P$ and $V_S$ can be more appropriately explained by a thinner ULVZ layer (about half as thick) with reductions in $V_P$ and $V_S$ of 10% and 30%, respectively (as illustrated in Figure 10). Synthetics for ULVZ thicknesses greater than 20 km (with $\delta V_P$=-10%, $\delta V_S$=-30%) show significant waveform complexities due to additional mode conversions and internal reflections associated with the large contrast in properties at the top of the ULVZ. The long-period WWSSN data analyzed thus far do not show the predicted complications due to $V_S$ reductions of 20% or more for such thicker layers. Therefore, to the first order, the solution figure of GH96 (i.e., Figure 4) would simply have a reduced range on the thickness scale to correspond to a ULVZ having an origin of partial melt.

Broadband data for the southwest Pacific geometry also possesses fairly simple $SKS$ and $SP_dKS$ waveforms (Figure 11). $SP_dKS$ lags behind $SKS$ in a systematic fashion (as in Figure 2). The data in Figure 11 are from a deep focus Fiji event and are used to illustrate some of the extreme trade-offs that exist for thin ULVZ structures. We systematically searched the ($\delta V_P$, $\delta V_S$, $\delta\rho$) parameter space for ULVZ structures that reproduce the behavior of the data of the event in Figure 11. Parameters explored include ULVZ thicknesses of 2, 5, 10, 15, and 20 km, $\delta V_P$=0,-2.5,-5, -10, -15, -20%, $\delta V_S$=0,-2.5,-5,-10,-15,-20,-30,-45%, and $\delta\rho$=0,+10,+20,+30,+60. The five best fitting models are shown in Figures 12a-12e along with the data (dashed traces); the ULVZ properties are given at the top. The synthetics are from the 1-D reflectivity method, which are not appropriate for path geometries possessing different ULVZ structures on the source and receiver sides of the $SP_dKS$ wave paths [e.g., GH96]. However, our intention is to focus on the range in possible solution structures due to model parameter trade-offs, which would also be present for any 2-D synthetics that attempt to accurately model the data.

In Figure 12a, a ULVZ with thickness of 10 km and ($\delta V_P$,$\delta V_S$,$\delta\rho$)=(-5%,-10%,0%) corresponding to a partial melt scenario agree well with the overall behavior of the data. Thinner layers having more extreme velocity and density perturbations similarly do well in matching the behavior (Figures 12b-12e). Figures 12b and 12c show synthetics for a ULVZ that is half as thick as that in Figure 12a (5 km), while Figures 12d and 12e correspond to a 2 km thick ULVZ. While subtle differences exist between the different synthetic runs, they all do equally well in predicting the observed waveforms given the uncertainties in the data (e.g., noise level, unaccounted for 3-D heterogeneity, etc). Figure 12 illustrates how increasing ULVZ property perturbations for decreasing layer thicknesses can, in principle, produce nearly identical synthetics. Thus ignoring conventional wisdom regarding feasible ULVZ velocity and density perturbations for likely lower mantle mineralogical assemblages significantly increases model space trade-offs. Another noteworthy point is that very thin ULVZ layers (i.e., much less than the dominant seismic wavelength) can significantly alter the wave field by trapping substantial $SP_dKS$ (and $SpKS$, etc.) energy, hence permitting identification of the anomalously thin layer. Here we make no effort to interpret the extremely anomalous ULVZ properties of possible solution structures (e.g., Figures 12d and 12e) but rather emphasize the model space uncertainties [see also, *Garnero et al.*, 1998].

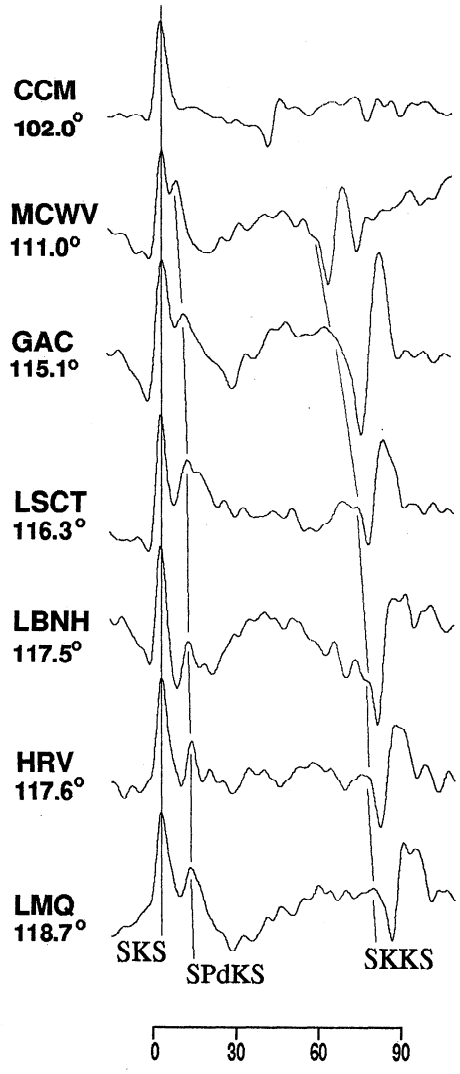


**Figure 11.** Broadband longitudinal component displacement observations (Fiji event of March 31, 1994), showing clear $SP_dKS$ arrivals with systematic moveout from $SKS$. Times and amplitudes are normalized to $SKS$.

We now explore the trade-off between ULVZ thickness and seismic properties in regards to how thick can a ULVZ layer be (with correspondingly less anomalous ULVZ properties) and still explain the anomalous observations. Figure 13 shows the results of synthetic tests for ULVZ thicknesses between 10 and 300 km, which are displayed at three epicentral distances. Figure 13a displays results for $\delta V_S$=$\delta V_P$=-2.5%, while Figure 13b has $\delta V_S$=$\delta V_P$=-5.0% (both have $\delta\rho$=0). The milder reduction of Figure 13a does not produce any significant $SP_dKS$ anomaly at 108° for any thickness, which is similar to results of *Garnero et al.* [1993] and GH96, which argued for the need of strong reductions at these small distances in order to produce the strong anomalies seen in the $SP_dKS$ anomalies for such correspondingly short $P_d$ segments. For the larger distances in Figure 13a, there is a slight change in $SP_dKS$ shape for ULVZ thickness (th) of 100 km and greater. This is due to the increasingly apparent effects of diffraction on the longer $P_d$ arcs. Figure 13b more clearly shows this trend: at

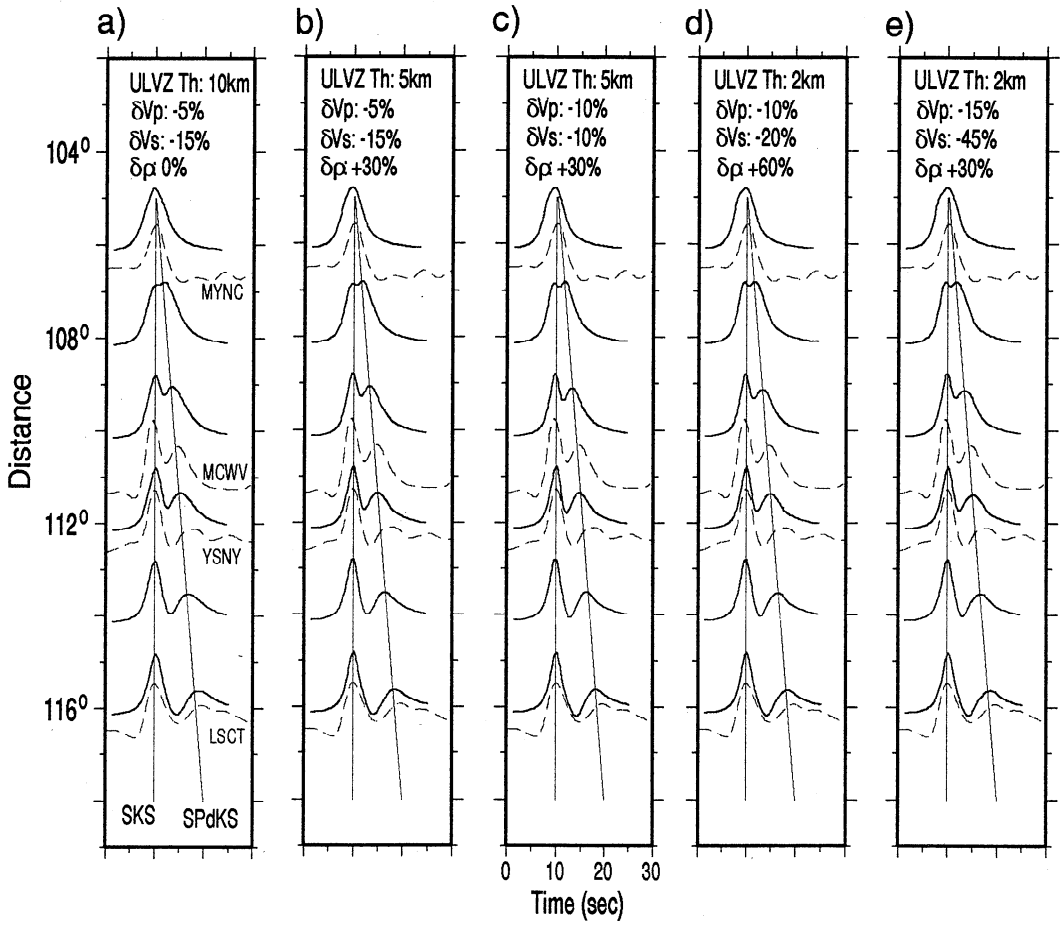


**Figure 12.** Reflectivity displacement synthetics (solid traces) for various ULVZ models, compared to observed recordings from the deep focus Fiji event of Figure 11, are displayed (dashed traces). ULVZ properties are listed at the top. All amplitudes and times are normalized to the *SKS* peak.

108°, th≥50 km all show similar $SP_dKS$ waveshape; thus the effect of thickening the ULVZ layer is only apparent up to th=50 km. At 112° and 116°, however, the cutoff thicknesses for $SP_dKS$ sensitivity are 100 and 200 km, respectively. The longer $P_d$ segments sample progressively higher up into the D″ layer. $SP_dKS$ modeling to date has focused on the shorter distance data (e.g., 108°-112°) where the interference between *SKS* and $SP_dKS$ is a strong diagnostic for detecting ULVZ anomalies. Hence, for such data, it is clear that milder ULVZ velocity reductions distributed over thicker zones can not explain the data (and in fact, thicknesses greater than 25-50 km make little difference in the waveforms for such mild anomalies). The strongest $SP_dKS$ anomalies of GH96 and also *Helmberger et al.* [1998] cannot be fit with the mild reductions of Figure 13, though such structures are in the model solution space for $SP_dKS$ data exhibiting only mild anomalies. Also present is the $S^PKS$ precursor to *SKS* (e.g., Figure 13, 112°), which has not been identified in data as of yet (this, of course, does not preclude the possibility of its existence). Nonetheless, some of the milder $SP_dKS$ anomalies (e.g., for CAR in Figure 3c) can contain such models in the solution space of possible ULVZ structures.

The top of the ULVZ has been parameterized as discontinuous from the overlying mantle in the previous synthetic calculations. Gradient ULVZ layers can also produce strong $SP_dKS$ anomalies and trade-off with discontinuous ULVZ structures having constant properties. Figure 14 displays synthetic seismogram profiles (solid traces) for ULVZ gradient models of various thicknesses, which are linear departures from PREM down to the CMB, with CMB $\delta V_P$ and $\delta V_S$ reductions of -10% and -30%, respectively. Also shown in Figure 14 is a synthetic profile for a 5 km thick discontinuous ULVZ having the same magnitude of reductions (see velocity-depth profiles above each seismogram panel). The dashed traces in each panel correspond to the 5 km thick constant property ULVZ for reference. Figure 14 displays two key features: (1) for thin ULVZ layers, there is a direct trade-off between gradient ULVZ structures and thinner discontinuous ULVZ structures (Figure 14b); and (2) thicker gradient structures with anomalous ULVZ CMB properties display anomalous waveform behavior not observed in the data (compare solid traces in Figures 14d and 14e with data in Figures 2 and 11). Thus thick gradient zones (i.e., > 20 km) are not likely to be in the solution space for modeling our anomalous $SP_dKS$ data. The same trade-off as shown in Figure 14 will exist for *PcP* and *ScP* data, though exact systematics of the extent of the trade-off are left for future work.

As mentioned earlier, increasing ULVZ density can add to $SP_dKS$ anomalies. Figure 15 further establishes some systematics in this regard. For three distances of 108°, 112°, and 116° (rows), four columns of various $\delta V_P$ and $\delta V_S$ reductions are displayed: columns 1 and 2 are for 1:1 $\delta V_P$ and

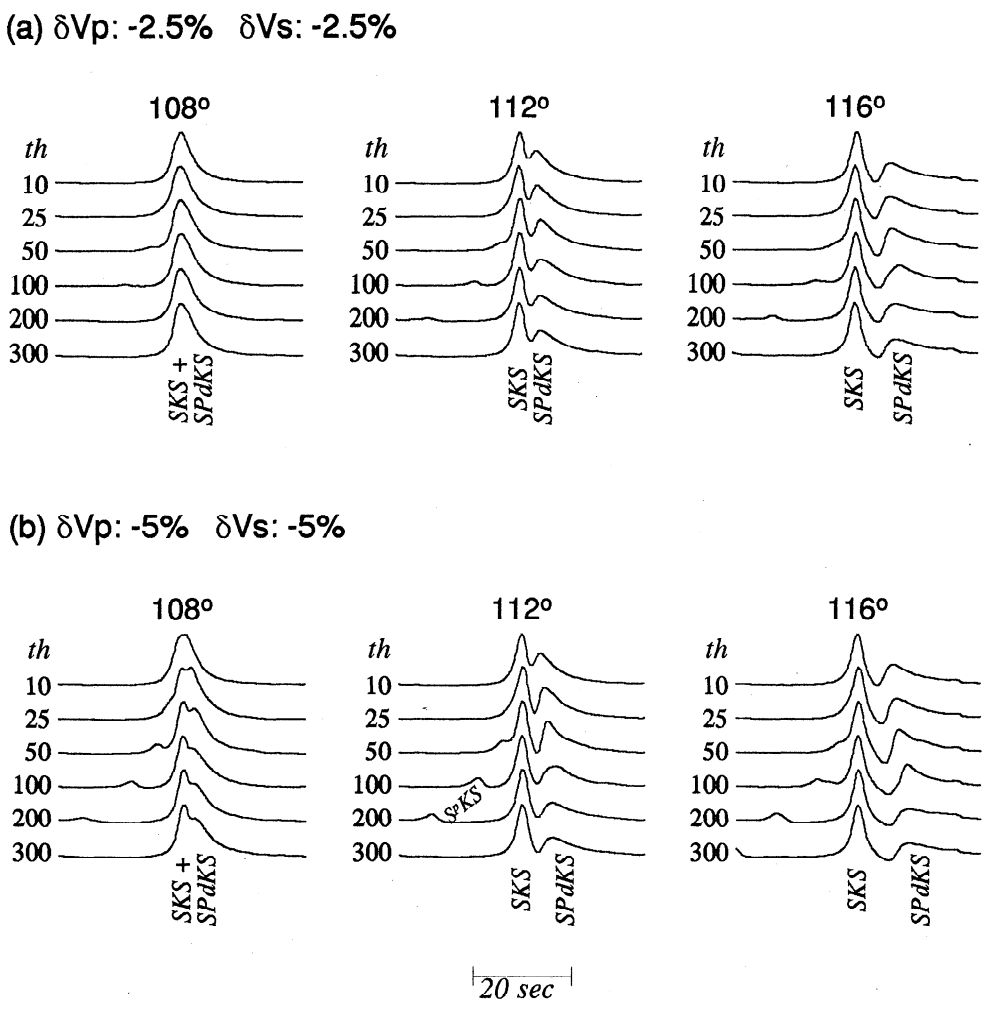


**Figure 13.** Reflectivity displacement synthetics at three distances are displayed for various ULVZ thicknesses (th, left column of numbers) for (a) $\delta V_P = \delta V_S = -2.5\%$ and (b) $\delta V_P = \delta V_S = -5.0\%$. All amplitudes and times are normalized to the *SKS* peak.

$\delta V_S$ reductions, while columns 3 and 4 have 3:1 reductions, corresponding to the partial melt hypothesis. Solid, dotted, and dashed traces correspond to ρ perturbations of 0%, +30%, and +60%, respectively. Seismograms from the most anomalous ULVZ structures (column 4 in this experiment) display heightened sensitivity to the strong density increases, with the $SP_dKS$ arrival much longer period than *SKS*, and a more delayed peak as well (due to increasing *SpKS* energy, as previously discussed). Again, the perturbations are most apparent at the shorter distances, where the $P_d$ segments have shorter diffraction distances. Our experiments show that the large ρ increases most effectively modulate *SKS*-$SP_dKS$ behavior when they are accompanied with large velocity reductions.

It is very conceivable that ultralow-velocities in a CMB boundary layer may be accompanied by high attenuation (low *Q*), especially in an environment of partial melt. Our preliminary synthetic tests indicate that extremely low *Q* can reduce $SP_dKS$ amplitudes. Figure 16 shows reflectivity synthetics for key distances where the *SKS*-$SP_dKS$ bifurcation occurs (108° and 110°) for a ULVZ with ($\delta V_P$,$\delta V_S$,δρ)=(-10%,-30%,0). Displacement synthetics are shown for two different *Q* models: that of PREM ($Q_{PREM}$: $Q_\mu$=312, $Q_K$=57822) and an ultralow Q model ($Q_{5,5}$: $Q_\mu$=5, $Q_K$=5). The $Q_{5,5}$ synthetics at both distances show reduced $SP_dKS$ amplitudes relative to *SKS*, while roughly preserving the $SP_dKS$-*SKS* time. Such *Q* effects could easily be mismapped into ULVZ velocity structure. The ULVZ structure produces a diffracted *SV* waves that appear more as a wave train of energy ringing in the ULVZ (top trace in each of Figures 16a and 16b), whereas the low *Q* model dampens out such energy. The inherent trade-off between *Q* and structure certainly deserves more attention in future studies.

## 4. Discussion

Previous ULVZ modeling efforts identified the presence of a ULVZ with strong $V_P$ reductions (10%) [see *Garnero et al.*, 1998]. A one-parameter modeling approach, i.e., keeping the $V_P$ reduction fixed and varying ULVZ thickness, reproduced anomalous $SP_dKS$-*SKS* separations, but with this approach, $SP_dKS$ amplitude variability was not well explained. Additional ULVZ variations in topography, $\delta V_S$ and δρ (in addition to $\delta V_P$), can further alter $SP_dKS$ amplitudes and times to agree with data. Nonuniqueness is present, however, due to limited wave propagation tools and data coverage, as well as

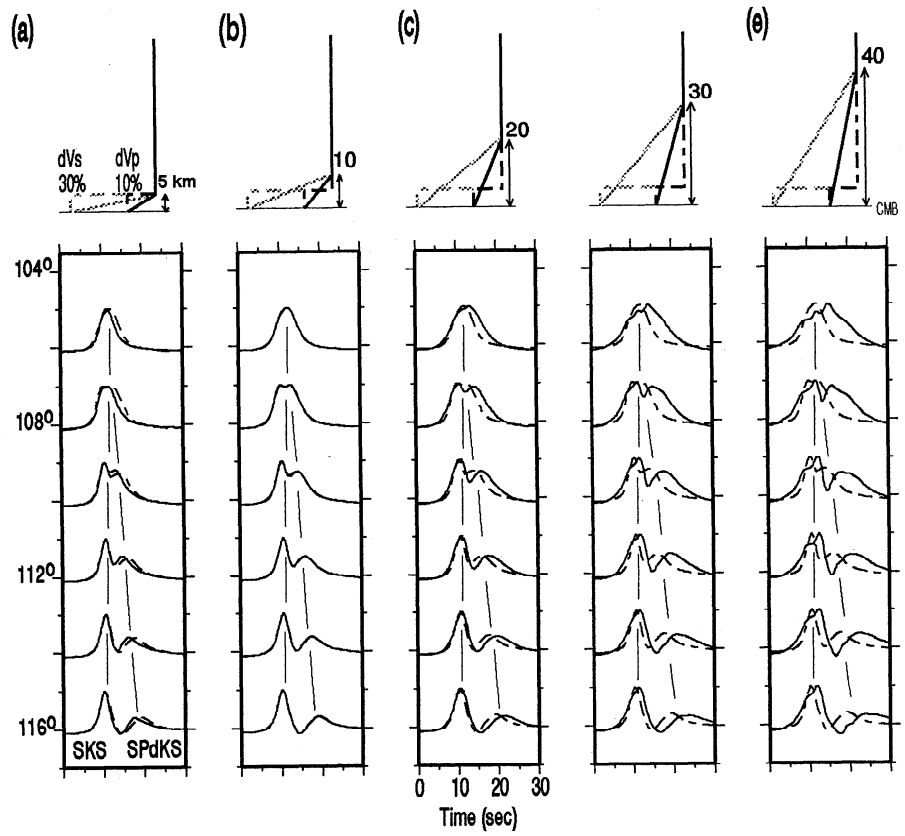


**Figure 14.** Reflectivity displacement synthetics for gradient ULVZ structures (solid traces) of thicknesses (a) 5, (b) 10, (c) 20, (d) 30, and (e) 40 km. Each panel is overlain with synthetics from a constant property ULVZ of thickness 5 km (dashed traces in each panel). All synthetics have CMB ($\delta V_P$,$\delta V_S$) reductions of (-10%,-30%). All amplitudes and times are normalized to the *SKS* peak.

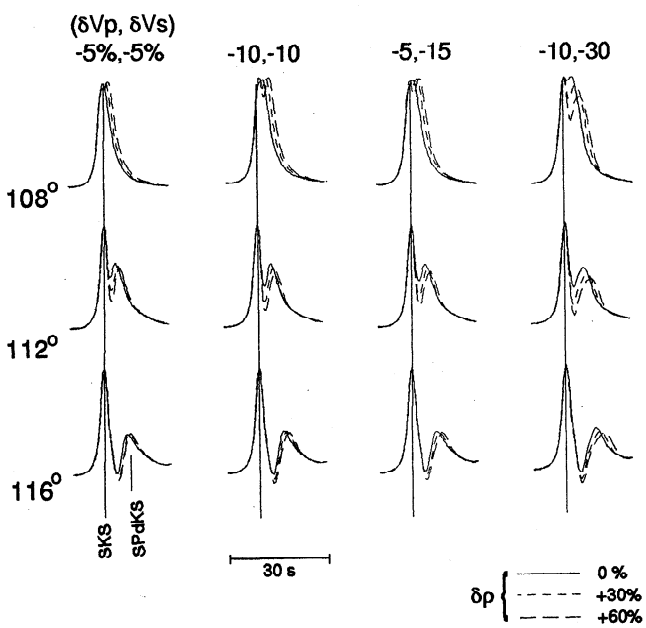


**Figure 15.** Reflectivity displacement synthetics at three distances (rows) computed for different ULVZ structures (top numbers), and for density perturbations of 0% (solid), +30% (dotted), and +60% (dashed). The large density increases modulate the *SKS-SP$_d$KS* behavior (see text for more details). All amplitudes and times are normalized to the *SKS* peak.

uncertainties in ULVZ properties, including gradients throughout the ULVZ, and also attenuation. Future work should include 3-D wave propagation experiments to further explore effects of ULVZ heterogeneity compared to topography.

If the origin of the ULVZ is due partial melt of mantle material [*Williams and Garnero*, 1996; *Holland and Ahrens*, 1997; *Vidale and Hedlin*, 1998], then a 3:1 $\delta V_S$:$\delta V_P$ reduction in the ULVZ is predicted. Using ($\delta V_P$,$\delta V_S$)=(-10%,-30%) results in waveform complexities for ULVZ thicknesses much greater than 20 km (Figure 9). Thus accommodating the partial melt scenario argues for a slightly thinner ULVZ in the southwest Pacific than presented in GH96 (maximum thickness 20 km as opposed to 40 km, for these values of velocity reductions).

The D″ discontinuity structure does not affect our analysis, since *SP$_d$KS* and *SKS* travel nearly identical mantle paths [e.g., see *Garnero et al.*, 1993], but nonetheless is probably intimately related to the small- and large-scale lower mantle dynamics which are most likely coupled to ULVZ variability. We also note that structure above the ULVZ is not constrained from *SP$_d$KS*-*SKS* analysis.

Strong lateral variations in ULVZ structure (topography and/or heterogeneity) exist at small length scales (<100 km). Such structure may be related to the cause of *PKP* precursors [e.g., *Haddon and Cleary*, 1974; *Bataille and Flatte*, 1988; *Vidale and Hedlin*, 1998] but may be difficult to separate from contributions from higher up above the CMB [*Hedlin et al.*,

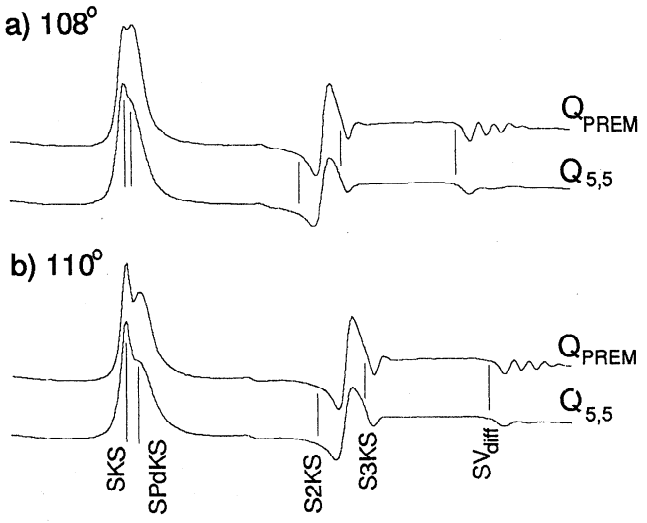


**Figure 16.** Reflectivity displacement synthetics for a ULVZ with ($\delta V_P$,$\delta V_S$) reductions of (-10%,-30%) at (a) 108° and (b) 110°. Quality factors (1/attenuation) for PREM (top trace) and for a low $Q$ model (bottom) trace are shown. All amplitudes and times are normalized to the *SKS* peak.

1997]. If the ULVZ is intimately related to lower mantle circulation patterns, then such small-scale perturbations may be dynamically linked to lower mantle heterogeneity occurring at short to intermediate scales in that region [e.g., *Garnero and Helmberger*, 1993; *Wysession et al.*, 1994; *Breger et al.*, 1998; *Vinnik et al.*, 1998]. Also, the apparent link of low velocities in the lower mantle and the existence of a ULVZ in the Pacific suggests the possibility of a relationship between mantle upwelling and the ULVZ (e.g., see *Wysession* [1996b] for a discussion on possible scenarios of mantle circulation patterns and their relationship to seismically detected lower mantle layering). In fact, Williams et al. (submitted manuscript, 1998) have noted the anomalously strong correlation between geographical locations of hotspots and ULVZ locations.

## 5. Conclusions

Strong variability in anomalous $SP_dKS$ travel time delays and amplitudes referenced to *SKS* imply short-scale variations in ULVZ properties. Deducing exact ULVZ properties is precluded at present due to significant trade-offs in properties, including $\delta V_P$, $\delta V_S$, $\delta\rho$, topography, gradients, and attenuation, as well as uncertainties in contribution to observed anomalies from the source side versus receiver side of path geometries. While much of our data can be explained by a ULVZ having reductions in $V_P$ (-10%), $V_S$ (-30%), possible increases in $\rho$, and variable topography, exact values for the elastic parameters, as well as ULVZ thickness, are impossible to ascertain due to these trade-offs. Invoking the partial melt explanation as the cause of the ULVZ results in reduced thicknesses for the ULVZ layer, e.g., the maximum thickness for the southwest Pacific study region is around 20 ± 5 km assuming ($\delta V_P$,$\delta V_S$,$\delta\rho$)=(-10%,-30%,+20%). This number increases (up to 40 km) if no shear velocity and density perturbations are included. Topographic and/or volumetric heterogeneity of the ULVZ probably exists at scale lengths less than 100 km. Further development of 2- and 3-D wave propagation methods in conjunction with larger collections of broadband data will facilitate reducing the various model trade-offs in future efforts.

**Acknowledgements.** We thank Steve Grand, Thorne Lay, Barbara Romanowicz, and Jeroen Ritsema for data, preprints, and helpful discussions, and we also thank the makers of GMT software [*Wessel and Smith*, 1991]. Reviews by Michael Wysession, Annie Souriau, and Peter Shearer improved the manuscript. This research was partially supported by NSF grant EAR-9896047.

## References

Aki, K., and P.G. Richards, *Quantitative Seismology, Theory and Methods*, W.H. Freeman, New York, 1980.

Aurnou, J.M., J.L Buttles, G.A., Neumann, and P.L. Olson, Electromagnetic core-mantle coupling and paleomagnetic reversal paths, *Geophys. Res. Lett., 23*, 2705-2708, 1996.

Bataille, K., and S. M. Flatte, Inhomogeneities near the core-mantle boundary inferred from short-period scattered *PKP* waves recorded at the global digital seismograph network, *J. Geophys. Res., 93*, 15,057-15,064, 1988.

Breger, L., B. Romanowicz, and L. Vinnik, Test of tomographic models of D″ using differential time data, *Geophys. Res. Lett., 25*, 5-8, 1998.

Choy, G. L., Theoretical seismograms of core phases calculated by frequency-dependent full wave theory, and their interpretation, *Geophys. J. R. Astron. Soc., 51*, 275-312, 1977.

Doornbos, D. J., and T. Hilton, Models of the core-mantle boundary and the travel times of internally reflected core phases, *J. Geophys. Res., 94*, 15,741-15,751, 1989.

Dziewonski, A. M., and D. L. Anderson, Preliminary reference Earth model (PREM), *Phys. Earth Planet. Inter., 25*, 297-356, 1981.

Fischer, K.M., J.M. Zaslow, E.J.Garnero, M.J. Fouch, M.E. Wysession, T.J. Clarke, and G.I. Al-eqabi, *SPdKS* constraints on a thin slow layer at the base of the mantle beneath the northwestern Pacific, *Eos Trans. AGU, 77* (48), F678, 1996.

Garnero E. J., and D. V. Helmberger, Travel times of *S* and *SKS*: Implications for three-dimensional lower mantle structure, *J. Geophys. Res., 98*, 8225-8241, 1993.

Garnero, E.J., and D.V. Helmberger, A very slow basal layer underlying large-scale low-velocity anomalies in the lower mantle beneath the Pacific: Evidence from core phases, *Phys. Earth Planet. Inter., 91*, 161-176, 1995.

Garnero, E.J., and D.V. Helmberger, Seismic detection of a thin laterally varying boundary layer at the base of the mantle beneath the central-Pacific, *Geophys. Res. Lett., 23*, 977-980, 1996.

Garnero E. J., S. P. Grand, and D. V. Helmberger, Low *P* wave velocity at the base of the mantle, *Geophys. Res. Lett., 20*, 1843-1846, 1993.

Garnero, E.J., J.S. Revenaugh, Q. Williams, T. Lay, and L.H. Kellogg, Ultralow velocity zone at the core-mantle boundary, in *Geophysical Monograph Series*, edited by M. Gurnis et al., AGU, Washington, D.C., in press, 1998.

Grand, S.P., R.D. van der Hilst, and S. Widiyantoro, Global seismic tomography: a snapshot of convection in the Earth, *GSA Today, 7*, 1-7, 1997.

Haddon, R. A. W., and J. R. Cleary, Evidence for scattering of seismic *PKP* waves near the mantle-core boundary, *Phys. Earth Planet. Inter., 8*, 211-234, 1974.

Hansen, U., and D.A. Yuen, Dynamical influences from thermal-chemical instabilities at the core-mantle boundary, *Nature, 334*, 237-240, 1988.

Hedlin, M.A.H., P.M. Shearer, and P.S. Earle, Waveform stacks of *PKP* precursors: Evidence for small-scale heterogeneity throughout the mantle, *Nature, 387*, 145-150, 1997.

Helmberger, D.V., E.J. Garnero, and X.-M. Ding, Modeling two-dimensional structure at the core-mantle boundary, *J. Geophys. Res., 101*, 13,963-13,972, 1996a.

Helmberger, D.V., L.-S. Zhao, and E.J. Garnero, Construction of synthetics for 2D structures, core phases, in *Proceedings of International School of Solid Earth Geophysics: Seismic Modeling of the Earth's Structure*, pp. 183-222, Soc. Ital. di Fis., Rome, Italy, 1996b.

Holland, K.G., and T.J. Ahrens, Melting of (Mg,Fe) $_2SiO_4$ in the core-mantle boundary of the Earth, *Science, 275*, 1623-1625, 1997.

Hong, T.-L., and D.V. Helmberger, Glorified optics and wave propagation in nonplanar structure, *Bull. Seismol. Soc. Am., 68*, 1313-1330, 1978.

Kellogg, L.H., and S.D. King, Effect of mantle plumes on the growth of D″ by reaction between the core and mantle, *Geophys. Res. Lett., 20*, 379-382, 1993.

Kind, R., and G. Müller, Computations of *SV* waves in realistic Earth models, *J. Geophys., 41*, 149-172, 1975.

Knittle, E. and R. Jeanloz, Simulating the core-mantle boundary: An experimental study of high-pressure reactions between silicates and liquid iron, *Geophys. Res. Lett., 16*, 609-612, 1989.

Lay, T., Q. Williams, and E.J. Garnero, The core-mantle boundary layer and deep earth dynamics, *Nature*, in press, 1998.

Manga, M., and R. Jeanloz, Implications of a metal-bearing chemical boundary layer in D″ on mantle dynamics, *Geophys. Res. Lett., 23*, 3091-3094, 1996.

Mori, J., and D.V. Helmberger, Localized boundary layer below the mid-Pacific velocity anomaly identified from a *PcP* precursor, *J. Geophys. Res., 100*, 20,359-20,365, 1995.

Müller, G., The reflectivity method: A tutorial, *J. Geophys., 58*, 153-174, 1985.

Olson, P., G. Schubert, and C. Anderson, Plume formation in the D″-layer and the roughness of the core-mantle boundary, *Nature, 327*, 409-413, 1987.

Revenaugh J.S., and R. Meyer, Seismic evidence of partial melt within a possibly ubiquitous low-velocity layer at the base of the mantle, *Science, 277*, 670-673, 1997.

Ritsema, J.E., E.J. Garnero, and T. Lay, A strongly negative shear velocity gradient and lateral variability in the lowermost mantle beneath the Pacific, *J. Geophys. Res., 102*, 20,395-20,411, 1997.

Ritzwoller, M.H., and E.M. Lavely, Three-dimensional seismic models of the Earth's mantle, *Rev. Geophys., 33*, 1-66, 1995.

Schweitzer, J., Untersuchung zur Geschwindigkeitsstruktur im unteren Erdmantel und im Bereich der Kern-Mantel-Grenze unterhalb des Pazifiks mit Scherwellen, Ph.D. thesis, 134 pp., Frankfurt Univ., Frankfurt, Germany, 1990.

Song, X.-D., and D.V. Helmberger, A *P* wave velocity model of Earth's core, *J. Geophys. Res., 100*, 9817-9830, 1995.

Su, W.-J., R.L. Woodward, and A.M. Dziewonski, Degree 12 model of shear velocity heterogeneity in the mantle, *J. Geophys. Res., 99*, 6945-6980, 1994.

Sylvander, M., and A. Souriau, Mapping S-velocity heterogeneities in the D″ region, from *SmKS* differential travel times, *Phys. Earth Planet. Inter., 94*, 1-21, 1996.

Sylvander, M., B. Ponce, and A. Souriau, Seismic velocities at the core-mantle boundary inferred from *P* waves diffracted around the core, *Phys. Earth Planet. Inter., 101*, 189-202, 1997.

Vidale, J.E., and M.A.H. Hedlin, Intense scattering at the core-mantle boundary north of Tonga: Evidence for partial melt, *Nature, 391*, 682-685, 1998.

Vidale, J.E., E.J. Garnero, and L.S.L. Kong, Sounding the base of the mantle by core reflections, *Eos Trans. AGU, 76* (46), Fall Meet. Suppl., F404, 1995.

Vinnik, L., L. Breger, and B. Romanowicz, Anisotropic structures at the base of the Earth's mantle, *Nature*, in press, 1998.

Wessel, P., and W.H.F. Smith, Free software helps map and display data, *Eos Trans. AGU, 72*, 441, 445-446, 1991.

Williams, Q., and E.J. Garnero, Seismic evidence for partial melt at the base of Earth's mantle, *Science, 273*, 1528-1530, 1996.

Wysession, M. E., Large-scale structure at the core-mantle boundary from diffracted waves, *Nature, 382*, 244-248, 1996a.

Wysession, M. E., Imaging cold rock at the base of the mantle: The sometimes fate of slabs?, in *Subduction: Top to Bottom, Geophys. Monogr. Ser.*, vol. 96, edited by G.E. Bebout et al., pp.369-384, AGU, Washington, D.C., 1996b.

Wysession, M. E., L. Bartko, and J. Wilson, Mapping the lowermost mantle using core-reflected shear waves, *J. Geophys. Res., 99*, 13,667-13,684, 1994.

Zhang, S., and D.A. Yuen, Various influences on the dynamics of mantle plumes in time-dependent 3-D compressible, spherical shell convection, *Phys. Earth Planet. Inter., 94*, 241-267, 1996.

E. J. Garnero, Berkeley Seismological Laboratory, University of California, 475 McCone Hall, Berkeley, CA 94720-4760. (email: eddie@seismo.berkeley.edu)

D. V. Helmberger, Seismological Laboratory, MS 252-21, California Institute of Technology, Pasadena, CA 91125. (email: helm@seismo.gps.caltech.edu)

(Received October 29, 1997; revised February 2, 1998; accepted February 18, 1998.)